ANL/ET/CP--80135
Conf-931079--16

Fatigue of Carbon and Low-Alloy Steels in LWR Environments*

O. K. Chopra, W. F. Michaud, and W. J. Shack

Energy Technology Division
Argonne National Laboratory
9700 South Cass Avenue
Argonne, Illinois 60439 USA

October 1993

To be published in the Proceedings of the 21st Water Reactor Safety Information Meeting, October 25–27, 1993, Bethesda, MD.

* Work supported by the Office of Nuclear Regulatory Research, U.S. Nuclear Regulatory Commission. FIN Nos. A22122 and A22562, Program Manager Dr. J. Muscara.

Fatigue of Carbon and Low-Alloy Steels in LWR Environments*

O. K. Chopra, W. F. Michaud, and W. J. Shack
Energy Technology Division
Argonne National Laboratory
Argonne, Illinois 60439

Abstract

Fatigue tests have been conducted on A106-Gr B carbon steel and A533-Gr B low-alloy steel to evaluate the effects of an oxygenated-water environment on the fatigue life of these steels. For both steels, environmental effects are modest in PWR water at all strain rates. Fatigue data in oxygenated water confirm the strong dependence of fatigue life on dissolved oxygen (DO) and strain rate. The effect of strain rate on fatigue life saturates at some low value, e.g., between 0.0004 and 0.001%/s in oxygenated water with ≈0.8 ppm DO. The data suggest that the saturation value of strain rate may vary with DO and sulfur content of the steel. Although the cyclic stress-strain and cyclic-hardening behavior of carbon and low-alloy steels is distinctly different, the degradation of fatigue life of these two steels with comparable sulfur levels is similar. The carbon steel exhibits pronounced dynamic strain aging, whereas strain-aging effects are modest in the low-alloy steel. Environmental effects on nucleation of fatigue crack have also been investigated. The results suggest that the high-temperature oxygenated water has little or no effect on crack nucleation.

1 Introduction

Plain carbon and low-alloy steels are used extensively in PWR and BWR steam supply systems as piping and pressure-vessel materials. The steels of interest in these applications include A106-Gr B and A333-Gr 6 for seamless pipe and A302-Gr B, A508-2, and A533-Gr B plate for pressure vessels. The ASME Code Section III (Division 1, Subsection NB) includes rules for the construction of Class 1 components in nuclear power plants. It recognizes fatigue as a possible mode of failure in pressure vessel steels and piping materials. The current Code design curves, specified in Figure I-90 of Appendix I to Section III, are based primarily on strain-controlled fatigue tests of small polished specimens in air at room temperature.[1] The Code design curves were obtained by decreasing the best-fit curves to the experimental data by a factor of 2 on stress or a factor of 20 on cycles, whichever was more conservative at each point. The factors were intended to account for uncertainties in translating the experimental data of laboratory test specimens to actual reactor components. The factor of 20 on cycles is the product of three subfactors: 2 for scatter of data (minimum to mean), 2.5 for size effects, and 4 for surface finish, atmosphere, etc.[2] "Atmosphere" was intended to reflect the effects of an industrial environment rather than the controlled environment of a laboratory. The effects of the coolant environment are not explicitly addressed in the Code design curves.

---

*Work supported by the Office of Nuclear Regulatory Research, U.S. Nuclear Regulatory Commission. FIN Nos. A22122 and A22562, Program Manager Dr. J. Muscara.

Recent fatigue strain vs. life (S/N) data from the U.S.[3-10] and Japan[11-13] illustrate potentially significant effects of the LWR environment on the fatigue resistance of carbon and low-alloy steels. Specimen lives in simulated LWR environments can be much shorter than for the corresponding tests in air. In some cases, failures were observed below the ASME Code fatigue design curve for components. These results raise the issue of whether the fatigue design curves in Section III are appropriate for the purposes intended and whether they adequately account for environmental effects on fatigue behavior. The factors of 2 and 20 applied to the mean-data curve may not be as conservative as originally intended.

Several key variables that influence environmental effects can be identified from the available S/N data. The results indicate that environmental effect on fatigue life can be significant when all of the following variables exceed threshold values: (a) sulfur content of the steel is >0.003 wt.%, (b) concentration of dissolved oxygen (DO) in the water is ≥0.1 ppm, and (c) loading rate during the tensile half of the fatigue cycle is ≤0.1 %/s. The actual threshold values for a specific variable may vary with material and environmental conditions. For example, a sulfur content of ≥0.007% may be needed for environmental effects at 0.1 ppm DO, whereas a sulfur content of ≥0.004% may be sufficient at 1 ppm DO. Other factors that also affect fatigue life include alloy composition/structure, temperature, applied strain, loading history, and surface pitting. A threshold value or condition may also exist for these variables, e.g., a minimum plastic strain is required for environmental effects. However, the existing S/N data base is inadequate to establish these thresholds.

At the very low levels of DO characteristic of PWRs or BWRs with hydrogen/water chemistry, environmental effects on fatigue life are modest at all temperatures and strain rates. Fatigue life decreases rapidly as DO increases over a narrow range of ≈0.1-0.3 ppm, but further increases up to 8 ppm cause only a modest decrease in life. In oxygenated water, fatigue life strongly depends on temperature and strain rate. At a given strain rate, fatigue life increases by a factor of 5 or more as the temperature is decreased from 288 to 200°C. For the same environment and strain range, fatigue lives can be decreased by a factor of ≈50 by reducing the strain rate from 0.1 to 0.0001%/s. Based on the existing S/N data, Argonne National Laboratory (ANL) has developed interim fatigue design curves that take into account temperature, DO level in the water, sulfur level in the steel, and strain rate.[14]

The existing S/N data on carbon and low-alloy steels are somewhat limited and do not cover the range of loading conditions found in actual reactor operation. The data do not extend over the range of strain rates normally encountered in service, e.g., some transients may have strain rates as low as 0.00001%/s. Extrapolation of available data to such low values would predict a reduction in fatigue life by a factor of >300. The relatively good service experience of carbon steel piping in BWRs, i.e., 288°C water with 0.2 ppm DO, suggests that the effect of strain rate on fatigue life must saturate at some level, although direct experimental observations of saturation are very limited. Furthermore, environmental effects on crack nucleation have been considered as a possible mechanism for the reduction in fatigue life.[11,12] High-sulfur steels are more susceptible because cracks can initiate at surface micropits that form near manganese sulfide (MnS) inclusions. Effects of crack nucleation are important at low strain ranges, where experimental data are not available. Virtually all data in oxygenated water are at relatively high strain ranges where fatigue life is dominated by crack propagation.

The S/N data from Japan, compiled in the data base JNUFAD* for "Fatigue Strength of Nuclear Plant Component," also indicate that environmental effects on fatigue life are greater for carbon steel than for low-alloy steel.[11] However, most low-alloy steels that have been investigated in JNUFAD are low-sulfur heats (<0.007 wt.%). It is likely that differences between carbon and low-alloy steels are caused by the sulfur content of the steels and that compositional or structural differences have only minor effects on fatigue life.

This paper presents the results from fatigue tests conducted on A106-Gr B carbon steel and A533-Gr B low-alloy steel under conditions where information is lacking in the existing S/N data base. The effect of various material and test variables, e.g., strain rate, DO, strain range, composition, and surface pitting, on fatigue life of carbon and low-alloy steels has been evaluated. One of the major objectives of this year's work was to confirm that high-cycle fatigue life is little affected by LWR environments even at lower strain rates.

2 Experimental

Low-cycle fatigue tests are being conducted on A106-Gr B carbon steel and A533-Gr B low-alloy steel with an MTS closed-loop electrohydraulic machine. The A533-Gr B material was obtained from the lower head of the Midland reactor vessel, which was scrapped before the plant was completed. The A106-Gr B material was obtained from a 508-mm-diameter schedule 140 pipe fabricated by the Cameron Iron Works, Houston, TX. The chemical compositions of the two materials are given in Table 1, and average room-temperature tensile properties are given in Table 2. Microstructures of the steels are shown in Fig. 1; carbon steel has a pearlitic structure, whereas the low-alloy steel consists of tempered bainite. Smooth cylindrical specimens with 9.5-mm diameter and 19-mm gage length were used for the fatigue tests.

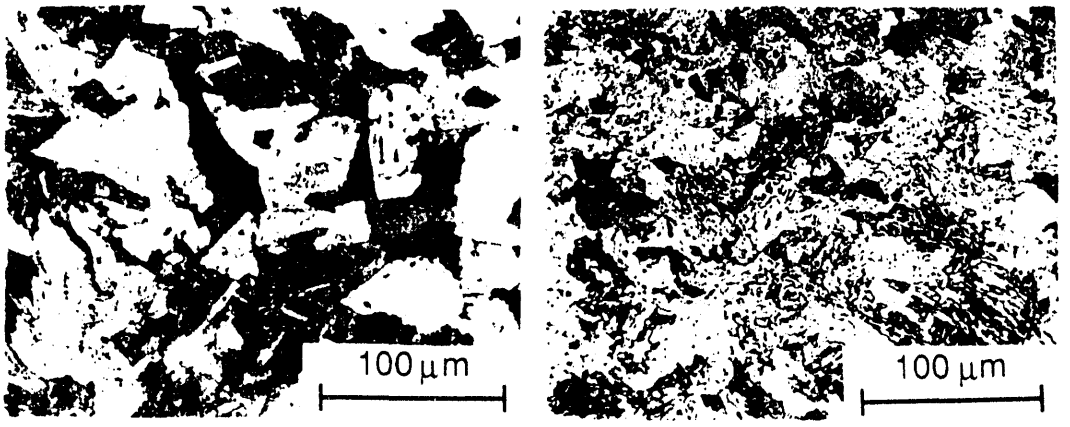

Figure 1. Microstructures of (a) A106-Gr B carbon steel and (b) A533-Gr B low-alloy steel

*Private communication from M. Higuchi, Ishikawajima-Harima Heavy Industries Co., Japan, to M. Prager of the Pressure Vessel Research Council (PVRC), January 1992. The old data base "FADAL" has been revised and renamed "JNUFAD."

Table 1. Chemical composition (wt.%) of ferritic steels used for fatigue tests

Material	Source/ Reference [a]	C	P	S	Si	Fe	Cr	Ni	Mn	Mo
					Carbon Steel					
A106–Gr B [b]	ANL	0.29	0.013	0.015	0.25	Bal	0.19	0.09	0.88	0.05
	Supplier	0.29	0.016	0.015	0.24	Bal	–	–	0.93	–
A106–Gr B	Terrell (7)	0.26	0.008	0.020	0.28	Bal	0.015	0.002	0.92	0.003
A333–Gr 6	Higuchi (11)	0.20	0.020	0.015	0.31	Bal	–	–	0.93	–
					Low-Alloy Steel					
A533–Gr B [c]	ANL	0.22	0.010	0.012	0.19	Bal	0.18	0.51	1.30	0.48
	Supplier	0.20	0.014	0.016	0.17	Bal	0.19	0.50	1.28	0.47
A533–Gr B	JNUFAD	0.19	0.020	0.010	0.27	Bal	0.13	0.60	1.45	0.52

[a] Reference number given within parentheses.
[b] Schedule 140 pipe 508–mm O.D. fabricated by Cameron Iron Works, Heat J–7201. Actual heat treatment not known.
[c] Hot-pressed plate 162 mm thick from Midland reactor lower head. Austenitized at 871–899°C for 5.5 h and brine quenched, then tempered at 649–663°C for 5.5 h and brine quenched. The plate was machined to a final thickness of 127 mm. The I.D. surface was inlaid with 4.8–mm weld cladding and stress relieved at 607°C for 23.8 h.

Table 2. Average room–temperature tensile properties of ferritic steels

Material	Reference[a]	Yield Stress (MPa)	Ultimate Stress (MPa)	Elongation (%)	Reduction in Area (%)
		Carbon Steel			
A106–Gr B	ANL	301	572	23.5	44.0
A106–Gr B	Terrell (7)	300	523	36.6	66.3
A333–Gr 6	Higuchi (10)	302	489	41.0	80.0
		Low-Alloy Steel			
A533–Gr B	ANL	431	602	27.8	66.6
A533–Gr B	JNUFAD	488	630	27.7	65.2

[a] Reference number given within parentheses.

All tests were conducted at 288°C with fully reversed axial loading (i.e., strain ratio R = –1) and a triangular or sawtooth wave form. Unless otherwise mentioned, the strain rate for the triangular wave and fast-loading half of the sawtooth wave was 0.4%/s. Tests in water were performed under stroke control where the specimen strain was controlled between two locations outside the autoclave. Tests in air were performed under strain control with an axial extensometer; specimen strain between the two locations used in the water tests was also recorded.

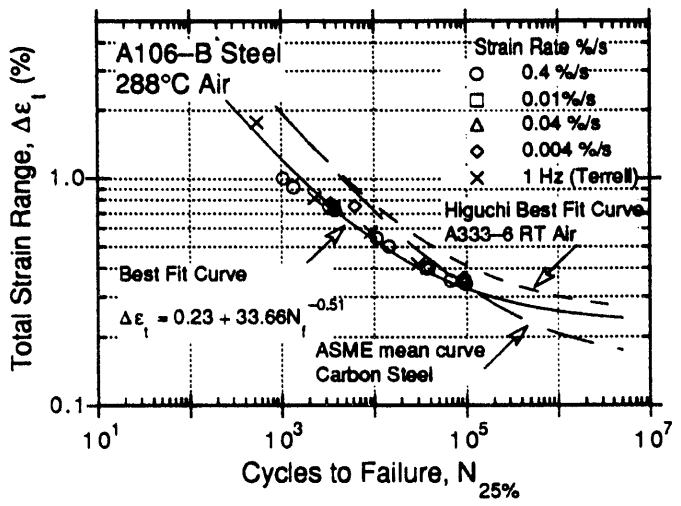

Figure 2.
Total strain range vs. fatigue life data for A106–Gr B steel in air

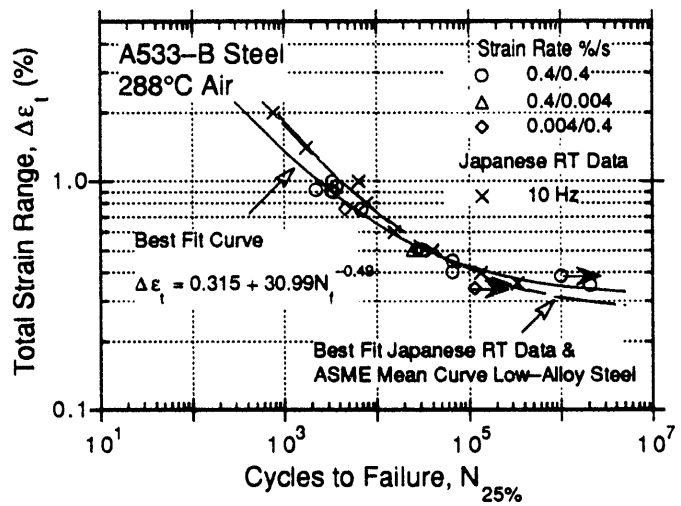

Figure 3.
Total strain range vs. fatigue life data for A533–Gr B steel in air

Information from the air tests was used to determine the stroke required to maintain constant strain in the specimen gage length for tests in water; stroke was gradually increased during the test to maintain constant strain in the specimen. A detailed description of the test facility and procedure have been presented elsewhere.[10]

3 Results

The fatigue results on A106–Gr B and A533–Gr B steels are summarized in Tables 3 and 4, respectively. The total strain range ($\Delta\varepsilon_t$) vs. fatigue life (N_{25}) curves for the carbon and low–alloy steels in air are shown in Figs. 2 and 3, respectively. Fatigue life is defined as the number of cycles required for a 25% decrease in tensile stress amplitude. Results from other investigations[7,11] on similar steels with comparable composition, in particular sulfur content, and the ASME Section III mean–data curves are also included in the figures. The results indicate that

Table 3. Fatigue test results for A106B steel

Test Number	Environ menta	Dissolved Oxygen (ppb)	pH at RT	Conducti- vity (μS/cm)	Tensile Rate[b] (%/s)	Comp. Rate[b] (%/s)	Stress Range (MPa)	Strain Range (%)	Life N_{25} (Cycles)	Pre exposure[c]
				Strain Control Tests						
1498	Air	–	–	–	0.4	0.4	1001.4	1.004	1,048	
1553	Air	–	–	–	0.4	0.4	921.1	0.757	3,253	
1615	Air	–	–	–	0.04	0.4	959.8	0.755	3,873	
1609	Air	–	–	–	0.004	0.4	1026.0	0.756	3,721	
1673	Air	–	–	–	0.004	0.4	1003.6	0.759	6,275	
1543	Air	–	–	–	0.4	0.4	818.2	0.502	14,525	
1638	Air	–	–	–	0.4	0.4	803.0	0.440	26,728	1
1636	Air	–	–	–	0.4	0.4	749.6	0.402	34,829	2
1619	Air	–	–	–	0.4	0.4	741.7	0.401	37,142	
1621	Air	–	–	–	0.01	0.4	787.1	0.403	38,128	
1550	Air	–	–	–	0.4	0.4	681.7	0.353	66,768	
1552	Air	–	–	–	0.4	0.4	680.6	0.352	93,322	
1644	Air	–	–	–	0.004	0.4	702.0	0.364	>95,000	
				Stroke Control Tests						
1546	Air	–	–	–	0.4	0.4	975.7	0.916	1,365	
1612	Air	–	–	–	0.004	0.4	1008.2	0.779	3,424	
1554	Air	–	–	–	0.4	0.4	896.8	0.730	3,753	
1548	Air	–	–	–	0.4	0.4	831.9	0.545	10,632	
1555	Air	–	–	–	0.4	0.4	676.3	0.343	98,456	
1547	PWR	8	6.7	23.26	0.4	0.4	1010.9	0.987	692	
1564	PWR	12	6.6	21.74	0.4	0.4	942.0	0.769	1,525	
1549	PWR	8	6.7	25.64	0.4	0.4	827.0	0.533	9,396	
1560	PWR	12	6.6	23.73	0.4	0.4	701.3	0.363	35,190	
1556	PWR	8	6.6	22.73	0.4	0.4	710.9	0.360	38,632	
1632	BWR	800	5.8	0.11	0.4	0.4	913.3	0.740	2,077	
1614	BWR	400	5.9	0.11	0.004	0.4	930.4	0.786	303	
1623	BWR	800	5.9	0.08	0.004	0.004	943.8	0.792	338	
1616	BWR	800	5.8	0.08	0.0004	0.4	912.8	0.799	153	
1620	BWR	900	5.9	0.11	0.00004	0.004	943.1	0.794	161	
1634	BWR	800	5.8	0.16	0.4	0.4	733.2	0.400	19,318	
1624	BWR	800	5.9	0.10	0.004	0.4	775.7	0.456	2,276	
1639	BWR	800	5.9	0.09	0.004	0.4	751.6	0.418	2,951	
1637	BWR	900	5.9	0.11	0.4	0.4	788.0	0.470	16,622	3
1643	BWR	800	6.0	0.11	0.004	0.4	698.5	0.363	>65,000	

[a] Simulated PWR water contains 2 ppm lithium and 1000 ppm boron.

[b] Values for stroke-control tests are approximate. Actual strain rates range between ±5% of the listed value.

[c] Preexposure conditions are as follows:

1. Prior to being tested in air, specimen was fatigued for 570 cycles in oxygenated water with 800 ppb DO at 0.46% strain range with sawtooth wave form, 0.004 and 0.4%/s strain rates in tension and compression.
2. Specimen oxidized in oxygenated water with 600 ppb DO for 100 h at 288°C.
3. Specimen was fatigued for 569 cycles in oxygenated water with 800 ppb DO at 0.46% strain range with sawtooth wave form, 0.004 and 0.4%/s strain rates in tension and compression.

Table 4. Fatigue test results for A533B steel

Test Number	Environ menta	Dissolved Oxygen (ppb)	pH at RT	Conducti- vity (μS/cm)	Tensile Rate[b] (%/s)	Comp. Rate[b] (%/s)	Stress Range (MPa)	Strain Range (%)	Life N_{25} (Cycles)	Pre exposure[c]
				Strain Control Tests						
1508	Air	–	–	–	0.4	0.4	910.9	1.002	3,305	
1515	Air	–	–	–	0.4	0.4	866.1	0.752	6,792	
1625	Air	–	–	–	0.004	0.4	887.7	0.757	4,592	
1629	Air	–	–	–	0.4	0.4	782.9	0.503	31,243	1
1505	Air	–	–	–	0.4	0.4	767.6	0.501	31,200	
1576	Air	–	–	–	0.004	0.4	805.8	0.503	28,129	
1590	Air	–	–	–	0.4	0.004	821.1	0.503	24,471	
1640	Air	–	–	–	0.4	0.4	710.9	0.402	65,880	
1517	Air	–	–	–	0.4	0.4	692.5	0.353	2,053,295	
1659	Air	–	–	–	0.004	0.4	656.2	0.343	>114,294	
				Stroke Control Tests						
1521	Air	–	–	–	0.4	0.4	889.4	0.910	3,219	
1523	Air	–	–	–	0.4	0.4	898.6	0.917	2,206	
1522	Air	–	–	–	0.4	0.4	905.4	0.899	3,419	
1524	Air	–	–	–	0.4	0.4	892.3	0.950	3,714	
1525	Air	–	–	–	0.4	0.4	743.6	0.452	65,758	
1538	Air	–	–	–	0.4	0.4	708.0	0.387	>1,000,000	
1526	DI	16	–	–	0.4	0.4	876.4	0.873	3,332	
1527	DI	17	6.0	–	0.4	0.4	752.8	0.493	10,292	
1528	DI	5	5.8	–	0.4	0.4	744.1	0.488	25,815	
1530	PWR	3	6.9	41.67	0.4	0.4	885.5	0.894	1,355	
1545	PWR	8	6.9	22.73	0.4	0.4	889.7	0.886	3,273	
1533	PWR	4	6.9	45.45	0.004	0.4	916.0	0.774	3,416	
1529	PWR	3	6.9	45.45	0.4	0.4	743.4	0.484	31,676	
1588	PWR	6	6.5	23.26	0.004	0.4	828.7	0.514	15,321	
1605	PWR	9	6.5	23.81	0.4	0.004	785.2	0.460	>57,443	
1539	PWR	6	6.8	38.46	0.4	0.4	694.8	0.373	136,570	
1542	PWR	6	6.6	27.03	0.4	0.4	631.8	0.354	>1,154,892	
1645	BWR	800	6.1	0.07	0.4	0.4	831.1	0.721	2,736	
1626	BWR	900	5.9	0.13	0.004	0.4	910.1	0.788	247	
1627	BWR	800	5.9	0.10	0.004	0.4	826.8	0.534	769	
1641	BWR	800	5.9	0.09	0.4	0.4	693.0	0.374	17,367	
1665	BWR	800	6.1	0.08	0.004	0.4	717.0	0.376	3,455	
1666	BWR	750	6.1	0.09	0.0004	0.4	728.4	0.376	>7,000	
1647	BWR	800	6.1	0.09	0.4	0.4	688.0	0.363	26,165	
1660	BWR	750	6.1	0.11	0.004	0.4	689.6	0.360	>83,024	
1649	BWR	700	6.3	0.08	0.4	0.4	673.4	0.352	28,710	
1652	BWR	700	6.1	0.09	0.4	0.4	638.1	0.328	56,923	
1655	BWR	750	6.1	0.10	0.4	0.4	567.6	0.298	>1,673,954	

[a] DI: Deionized water.
Simulated PWR water contains 2 ppm lithium and 1000 ppm boron.

[b] Values for stroke-control tests are approximate. Actual strain rates are ±5% of the listed value.

[c] Preexposure conditions are as follows:
1. Specimen oxidized in oxygenated water with 600 ppb DO for 100 h at 288°C.

for both steels, strain rate has no effect on fatigue life in air. The data for A106–Gr B steel are in excellent agreement with results obtained by Terrell[6,7] on A106–Gr B steel, but are lower by a factor of ≈5 than those obtained by Higuchi and Iida[11] on A333–Gr 6 steel. Also, the data for A106–Gr B steel are below the ASME mean–data curve for carbon steel at room temperature at high strain ranges (by a factor of 3), but are above the ASME mean curve at low strain ranges. The combined data from the present study and those obtained by Terrell for A106–Gr B steel may be expressed by the relationship

$$\Delta\varepsilon_t = 0.230 + 33.66 N_{25}^{-0.51}. \quad (1)$$

The results for A533–Gr B steel show good agreement with the JNUFAD data on A533–Gr B steel and the ASME mean–data curve for low–alloy steel at room temperature. The data for A533–Gr B steel may be expressed by the relationship

$$\Delta\varepsilon_t = 0.315 + 30.99 N_{25}^{-0.49}. \quad (2)$$

3.1 Alloy Composition

The cyclic–hardening behavior of carbon and low–alloy steels is significantly different. Plots of cyclic stress range vs. fatigue cycles for A106–Gr B and A533–Gr B steels tested in air at 288°C and a total strain range of ≈0.75% are shown in Figs. 4 and 5, respectively. Cyclic strain–hardening of the steels is consistent with their microstructure. The A106–Gr B steel, with a pearlitic structure and low yield stress, exhibits rapid hardening during the initial 100 cycles of fatigue life. The extent of hardening increases with applied strain range. In addition, the A106–Gr B carbon steel also exhibits dynamic strain aging, a time–dependent phenomenon caused by interstitial elements dissolved in the ferrite matrix. Consequently, cyclic stress of carbon steel increases significantly with decreasing strain rate, although its fatigue life is not affected (Fig. 4). In contrast, the A533–Gr B low–alloy steel consists of a tempered bainitic structure, has a relatively high yield stress, and shows little or no initial hardening (Fig. 5). At low strain ranges, the A533–Gr B steel shows cyclic softening during the initial 100 cycles of fatigue life (Fig. 6). Because of its tempered bainitic structure, the low–alloy steel exhibits little or no dynamic strain aging.

The cyclic stress vs. strain curves for A106–Gr B and A533–Gr B steels at 288°C are shown in Figs. 7 and 8, respectively; cyclic stress corresponds to the value at half life. The results for A106–Gr B steel show excellent agreement with the data obtained by Terrell.[7] The total strain range $\Delta\varepsilon_t$ (%) can be expressed in terms of the cyclic stress range (MPa) with the equation obtained by Terrell at 288°C:

$$\Delta\varepsilon_t = \frac{\Delta\sigma}{1907.8} + \left(\frac{\Delta\sigma}{1010.4}\right)^{11.55}. \quad (3)$$

The best–fit stress vs. strain curve for A533–Gr B steel is represented by

$$\Delta\varepsilon_t = \frac{\Delta\sigma}{1965.0} + \left(\frac{\Delta\sigma}{956.0}\right)^{11.10}. \quad (4)$$

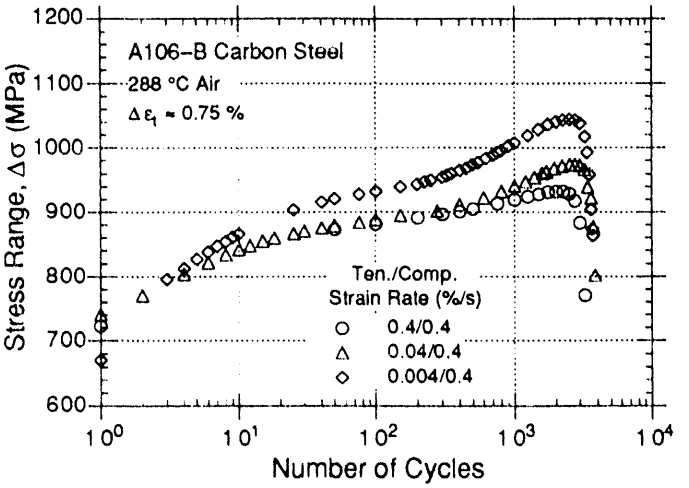

Figure 4.
Effect of strain rate on cyclic strain-hardening behavior of A106–Gr B steel in air at 288°C

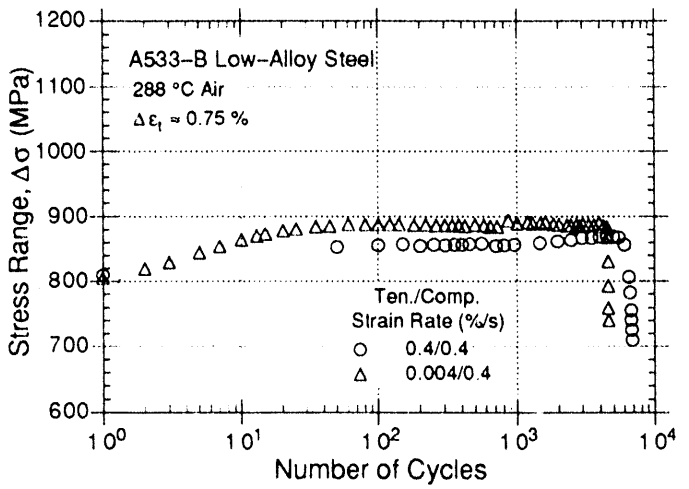

Figure 5.
Effect of strain rate on cyclic strain-hardening behavior of A533–Gr B steel in air at 288°C

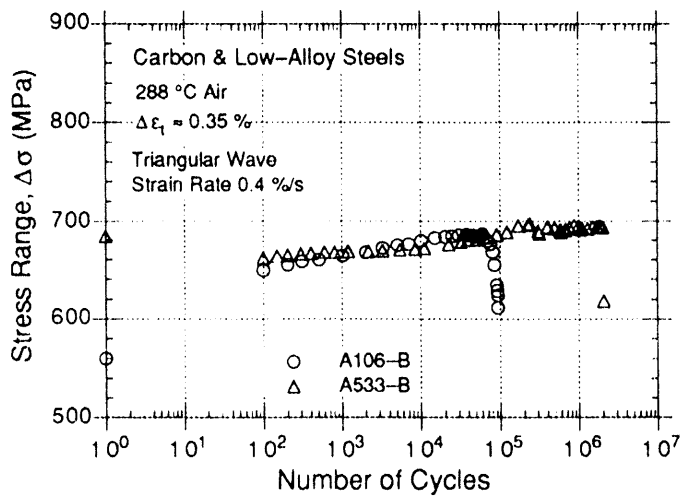

Figure 6.
Cyclic strain-hardening behavior of A106–Gr B and A533–Gr B steels at 0.35% total strain range and 0.4 %/s strain rate in air

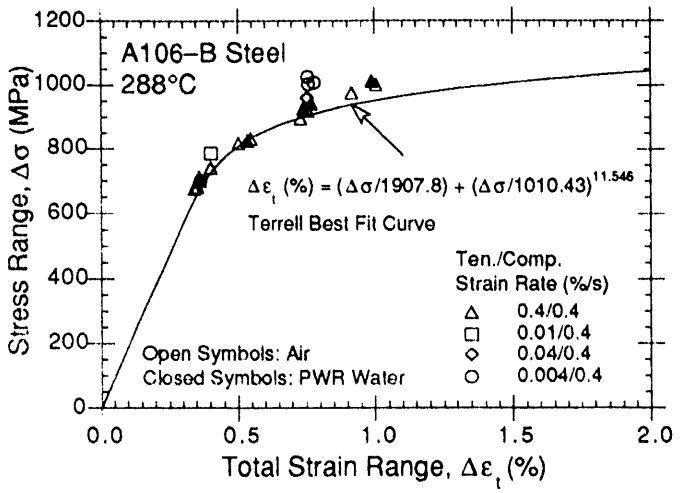

Figure 7.
Cyclic stress–strain curve for A106–Gr B steel at 288°C in air and water environments

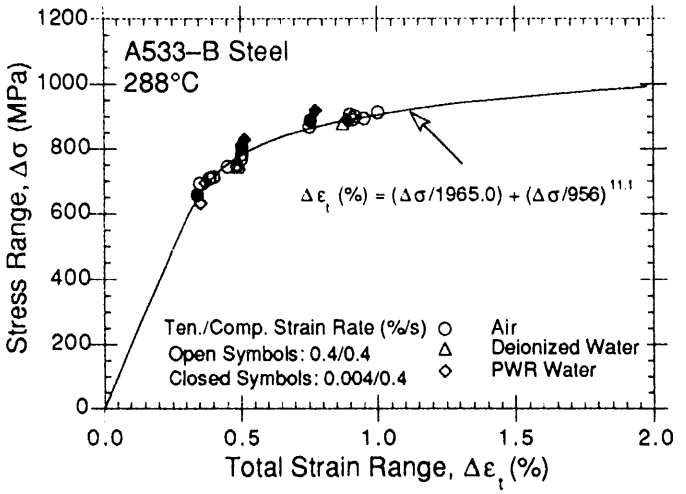

Figure 8.
Cyclic stress–strain curve for A533–Gr B steel at 288°C in air and water environments

The effect of strain rate on the cyclic stress–strain curve is quite pronounced in A106–Gr B carbon steel because of dynamic strain aging of the material, whereas strain rate has only a modest effect on the cyclic stress–strain curve for A533–Gr B low–alloy steel. For both steels, the oxygenated water environment has no effect on the cyclic stress–strain behavior.

Crack propagation behavior is also different for the carbon and low–alloy steels. Micrographs of fatigue cracks along longitudinal sections of the A106–Gr B and A533–Gr B steel specimens are shown in Fig. 9. In the carbon steel, fatigue cracks propagate preferentially along the soft ferrite grains. The low–alloy steel exhibits a typical straight fatigue crack propagating normal to the stress axis.

The surface oxide films that develop on the specimen surfaces tested in air or oxygenated water environments are not significantly different in the carbon or low–alloy steels. Micrographs of the gage surface of the steels tested in air and simulated PWR and BWR water are shown in Fig. 10. In general, the specimens tested in air show slight discoloration, while

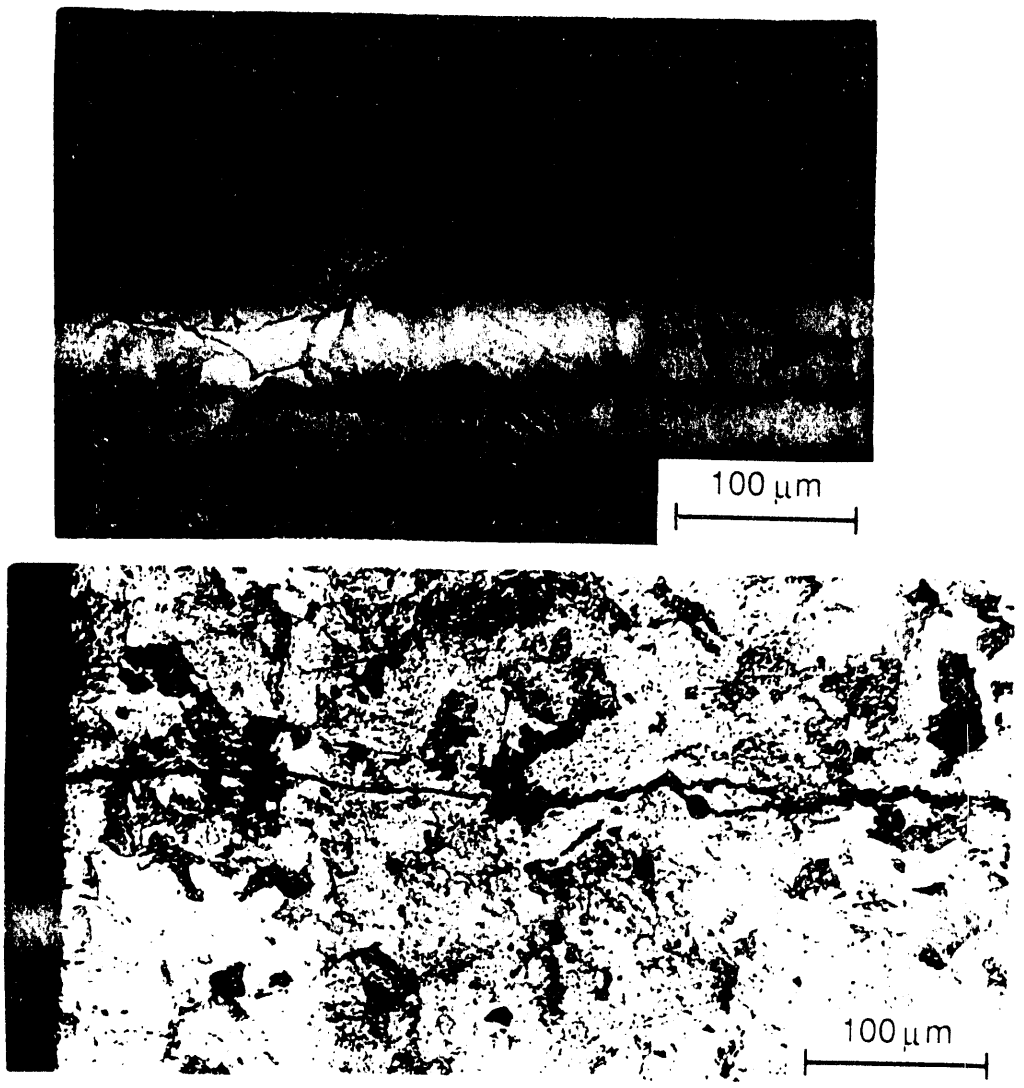

Figure 9. Micrographs of typical fatigue cracks along longitudinal sections of A106–Gr B carbon steel and A533–Gr B low–alloy steel specimens

the specimens tested in oxygenated water develop a gray/black corrosion scale and are covered with surface deposits. The specimens tested at high DO levels (0.8 ppm) also showed patches of loose brown/red deposit. X-ray diffraction analysis of the surfaces indicated that for both steels, the corrosion scale is primarily magnetite (Fe_3O_4) in simulated PWR water but also contains some hematite (Fe_2O_3) after exposure to oxygenated water containing ≈0.8 ppm DO.

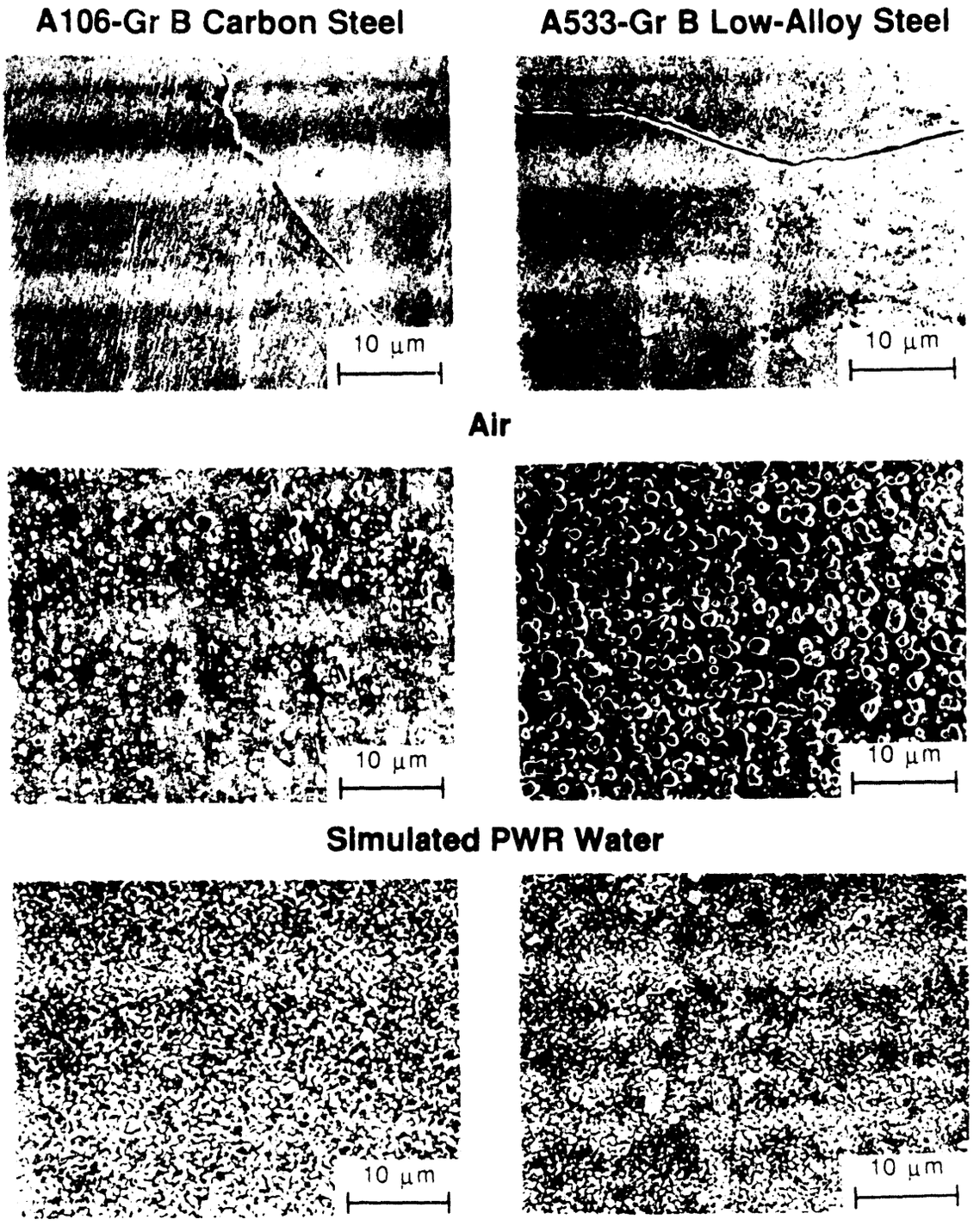

Figure 10. Micrographs of gage surface of A106–Gr B carbon steel and A533–Gr B low–alloy steel tested in different environments at 288°C

3.2 Simulated PWR Environment

The total strain range vs. fatigue life plots for A106–Gr B and A533–Gr B steels in simulated PWR water containing <10 ppb DO, 1000 ppm boron, and 2 ppm lithium are shown in Figs. 11 and 12, respectively. The results indicate a marginal effect of PWR water on fatigue life at high strain ranges. For both steels, fatigue lives in PWR water are lower by a factor of up to 2 than those in air at a strain range >0.5%. Fatigue lives in water and air environments are comparable at a strain range <0.5%. Limited data on A533–Gr B steel indicate that a decrease in the strain rate by two orders of magnitude does not cause an additional decrease in fatigue life. The results for A106–Gr B steel are consistent with the data obtained by Terrell[7] in simulated PWR water where no noticeable effect of strain rate or environment on fatigue life was observed (Fig. 11). The results are also consistent with the data of Iida et al.[12] and Prater and Coffin,[15,16] in which the effects of environment were minimal at DO levels of <100–200 ppb.

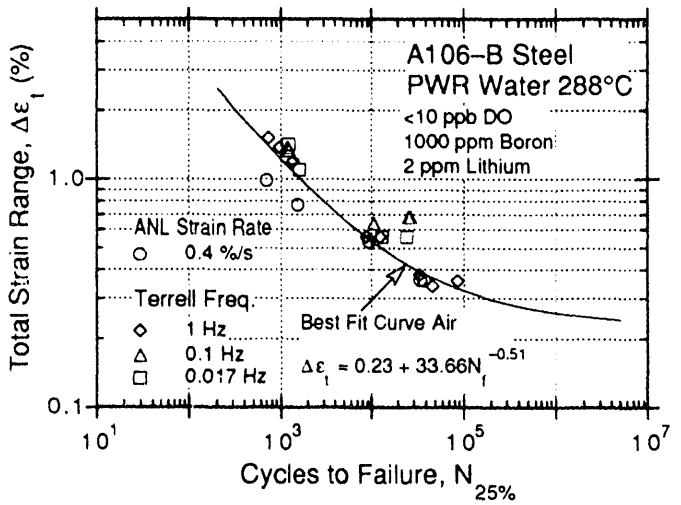

Figure 11.
Total strain range vs. fatigue life data for A106–Gr B steel in PWR water at 288°C

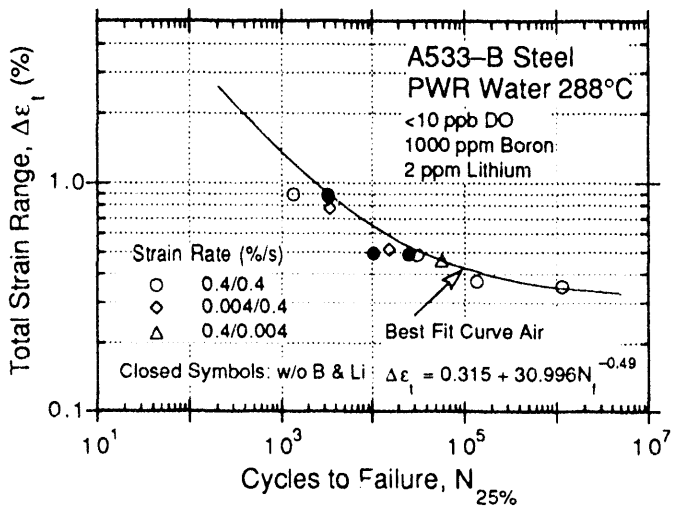

Figure 12.
Total strain range vs. fatigue life data for A533–Gr B steel in PWR water at 288°C

3.3 Oxygenated Water

Environmental effects are significant at high DO levels. The total strain range vs. fatigue life plots for A106–Gr B and A533–Gr B steels in oxygenated water containing ≈0.8 ppm DO are shown in Figs. 13 and 14, respectively. For A106–Gr B steel, fatigue tests were conducted at a total strain range of ≈0.75% with a sawtooth wave form and tensile strain rate between 0.4 and 0.00004%/s; the compressive strain rate for most tests was 0.4%/s. The results indicate that fatigue life decreases rapidly with decreasing strain rate and saturates at a strain rate between 0.001 and 0.0004%/s. Compared with tests in air, fatigue life in oxygenated water is lower by factors of 2, 10, and 20 at strain rates of 0.4, 0.004, and 0.0004%/s, respectively. A further decrease in strain rate to 0.00004%/s does not cause additional decrease in fatigue life. The relative reduction in fatigue life at total strain range of 0.75 or 0.4% are the same. The results also indicate that only the slow tensile–strain cycle is responsible for environmentally assisted reduction in fatigue life. Two fatigue tests on A106–Gr B steel at a strain range of ≈0.75%, one with a sawtooth wave form (i.e., 0.004 and 0.4%/s strain rates, respectively, during the tensile

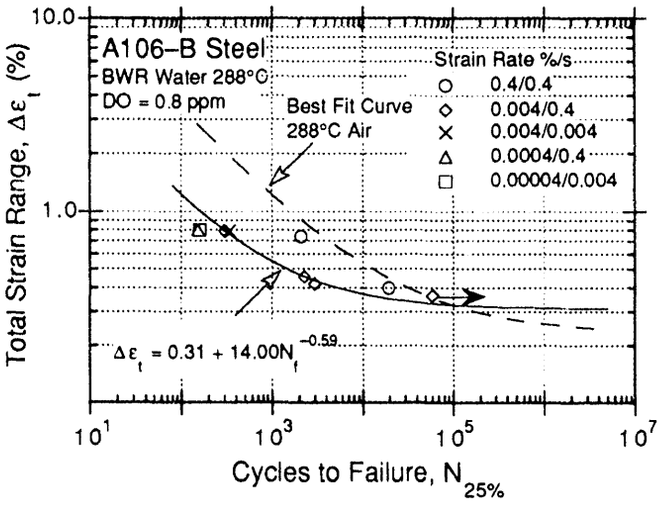

Figure 13.
Total strain range vs. fatigue life data for A106–Gr B steel in high–oxygen water at 288°C

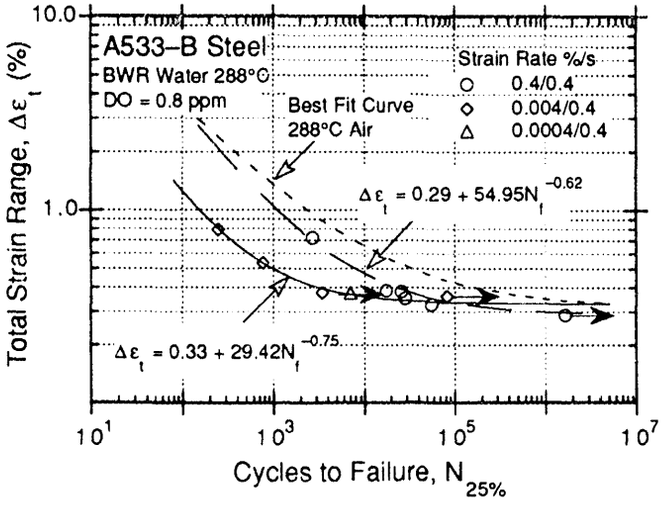

Figure 14.
Total strain range vs. fatigue life data for A533–Gr B steel in high–oxygen water at 288°C

and compressive half of the strain cycle) and the other with a triangle wave form (i.e., 0.004%/s constant strain rate), show identical fatigue lives (Fig. 13).

The low-alloy A533-Gr B steel shows an identical behavior. For similar test conditions, the absolute values of fatigue life for A533-Gr B low-alloy steel are comparable to those for A106-Gr B carbon steel. However, because life in air for A533-Gr B steel is greater than that for A106-Gr B steel, the relative reduction in life for the low-alloy steel is larger than that for carbon steel. This is particularly true at low strain range (0.4%), where even at the high strain rate fatigue life is a factor of 10 lower than in air (Fig 14).

3.4 Strain Rate

Fatigue data in oxygenated water reveal significant reductions in fatigue life and a strong dependence on strain rate. Although the microstructures and cyclic-hardening behaviors of the A106-Gr B carbon steel and A533-Gr B low-alloy steel are significantly different, there is little or no difference in environmental degradation of fatigue life of these steels. The relative fatigue lives of several heats of carbon and low-alloy steels with varying sulfur content are plotted as a function of strain rate in Figs. 15 and 16. Relative fatigue life is the ratio of life in water and life of that specific heat in air.

The results indicate that the reduction in fatigue life depends not only on strain rate but also on DO in the environment and sulfur content in the steel. Environmental effects increase with decreasing strain rates and increasing levels of DO and sulfur. For example, the maximum reduction in fatigue life for the A106-Gr B and A333-Gr 6 carbon steels with similar sulfur content is a factor of 2 at $\leq$0.05 ppm DO and a factor of 50 or more at 8 ppm DO. Fatigue lives at intermediate values of DO are between these limits.

However, the data obtained on A516 carbon steel (0.033 wt.% sulfur) by General Electric Co. (GE) in a test loop at the Dresden 1 reactor[3] show a different trend. For this steel, the reduction in fatigue lives at 0.2 ppm DO (shown as square data points in Fig. 15) is a factor of $\approx$2 greater than that for the A106-Gr B steel at 0.8 ppm DO and for A333-Gr 6 steel at 0.2 ppm DO. The difference may be attributed to the higher sulfur content in the A516 steel. Similar effects of DO and sulfur content are observed for the low-alloy steels. The results also indicate that for both steels, the effect of strain rate on fatigue life saturates at a value between 0.001 and 0.0004%/s; actual value may vary with DO and sulfur content.

Another factor that may influence environmental effects is wave shape. Fatigue tests on the A516 steel were conducted with a trapezoidal wave form instead of the sawtooth or triangular wave forms used in the ANL and Japanese studies. The trapezoidal wave form consists of hold periods at peak tensile and compressive strains. It is likely that in addition to the slow tensile strain rate, the tensile hold period also decreases fatigue life. Hold-time fatigue tests are in progress to establish the effects of wave shape.

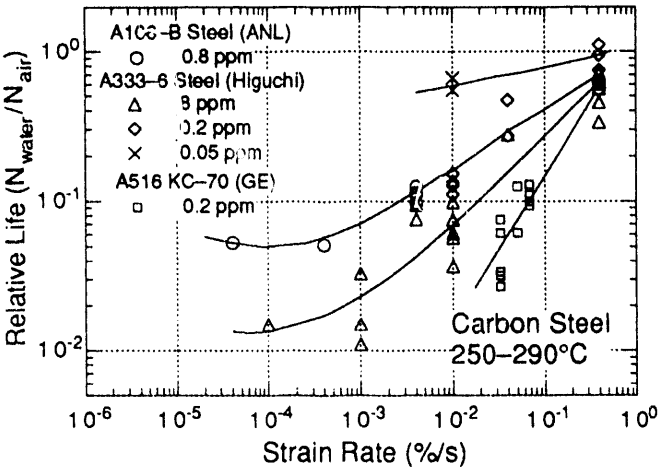

Figure 15.
Relative fatigue life of A106-Gr B carbon steel at different levels of dissolved oxygen and strain rates

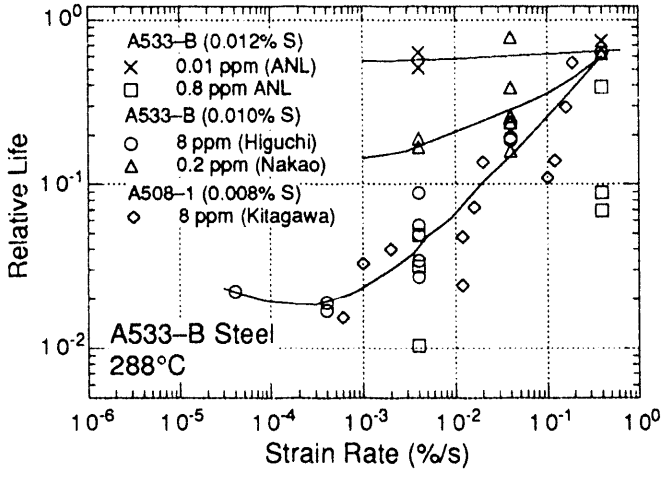

Figure 16.
Relative fatigue life of A533-Gr B low-alloy steel at different levels of dissolved oxygen and strain rates

3.5 Strain Range

The fatigue data in oxygenated water show a distinct threshold for the value of strain range for environmental effects. This threshold for the ANL heats of carbon and low-alloy steels appears to be at 0.36%; fatigue tests on A106-Gr B and A533-Gr B steels at ≈0.36% strain range, ≈0.8 ppm DO, and 0.004%/s tensile strain rate did not fail even after 65,000 and 83,000 cycles, respectively (Figs. 13 and 14). For the carbon steel, the fatigue strain range vs. life curves in air and water environments cross over at low strain ranges, i.e., fatigue life in water is longer than that in air. This apparently different fatigue S/N behavior is not due to the water environment. It is caused by dynamic strain aging of carbon steels and is observed in Fig. 13 because of the difference in strain rate for the tests in air and water environments. The S/N curve in air is based on tests at 0.4%/s strain rate, while the S/N curve in water represents fatigue tests at a slower strain rate of 0.004%/s. For a specific strain range, fatigue tests in water at slower strain rate show greater dynamic strain aging, higher cyclic stress, lower plastic strain range, and longer life.

3.6 Crack Nucleation

The reduction in fatigue life of carbon and low-alloy steels in oxygenated water may be caused by environmental effects on crack propagation and also on crack nucleation. The fatigue crack growth behavior of these steels in high-temperature oxygenated water and the effects of sulfur content and loading rate are well known.[17-24] The dissolution of MnS inclusions changes the water chemistry near the crack tip, making it more aggressive. This results in enhanced crack growth rates because either (a) the dissolved sulfides decrease the repassivation rate, which increases the amount of metal dissolution for a given oxide rupture rate; or (b) the dissolved sulfide poisons the recombination of H atoms liberated by corrosion, which enhances H uptake by the steel at the crack tip.

The water environment may also enhance crack nucleation. For example, corrosion pits or cavities produced by dissolution of MnS inclusions can act as sites for nucleation of fatigue cracks.[25,26] All specimens tested in air or water environments contained several secondary cracks, particularly those tested at high strain ranges. A detailed examination of the gage surfaces of the specimens was conducted to investigate the role of high-temperature oxygenated water on fatigue crack nucleation. The presence of surface deposits often impedes the examination. Consequently, the specimens were descaled with an electrolyte of 2 g hexamethylene tetromine in 1000 cm^3 of 1 N HCl. Micrographs of the gage surface of an A106-Gr B specimen before and after descaling are shown in Fig. 17. The descaled specimens show many details that were hidden by the oxide scale and/or deposits. Also, the descaled specimens show many more cracks that are not visible on the oxidized surface.

All specimens tested in water showed surface micropitting. These pits form either by corrosion of the material in oxygenated water or by selective dissolution of MnS or other inclusions. Typical examples of corrosion pits on A106-Gr B and A533-Gr B steel specimens are shown in

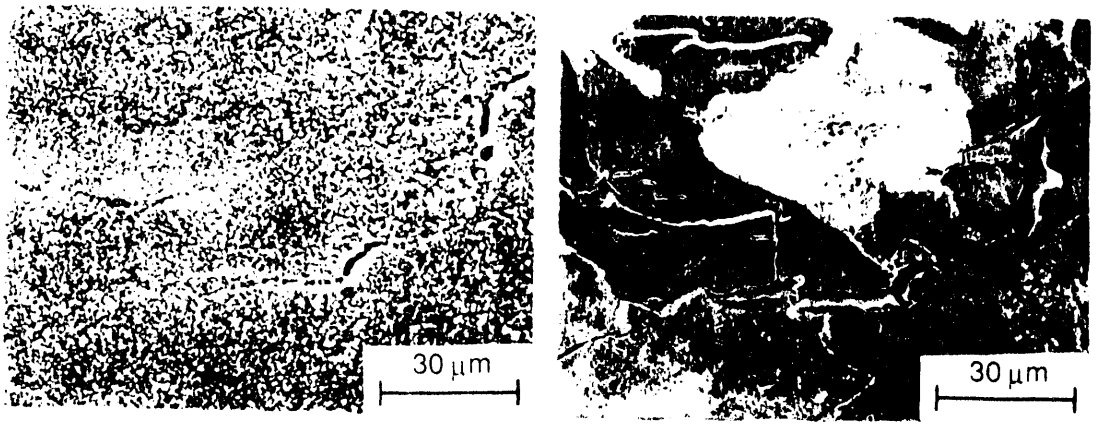

Figure 17. Micrographs of gage surfaces of A106-Gr B carbon steel specimens (a) before and (b) after descaling

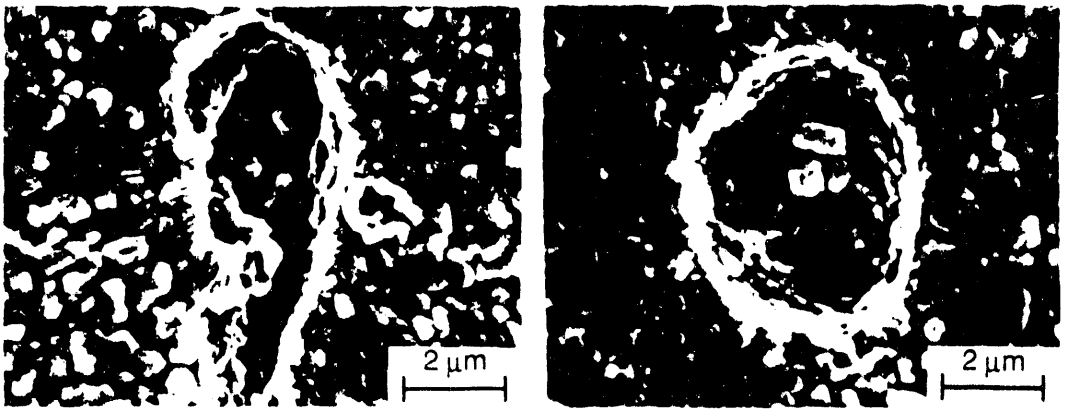

(a) (b)

Figure 18. Typical examples of micropits on the surface of (a) A106-Gr B carbon steel and (b) A533-Gr B low-alloy steel specimens tested in oxygenated water at 288°C

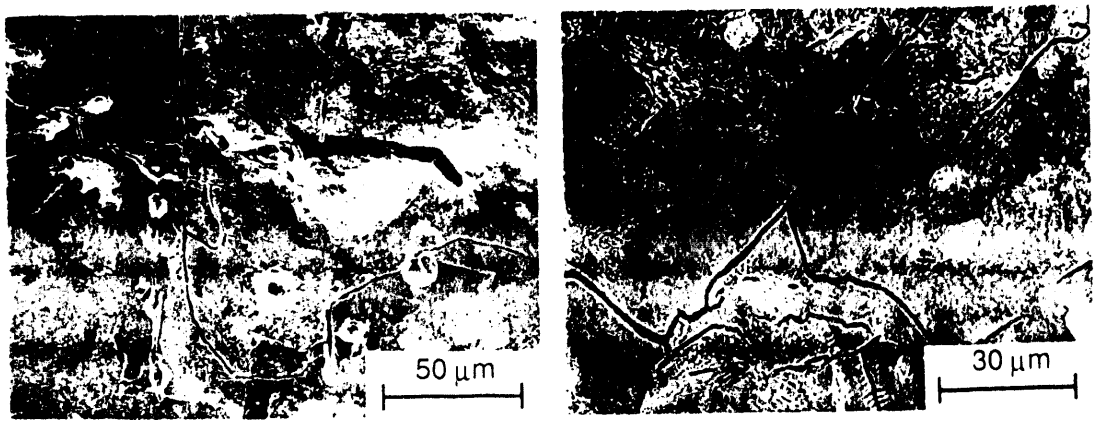

(a) (b)

Figure 19. Secondary fatigue cracks on the descaled surface of (a) A106-Gr B carbon steel and (b) A533-Gr B low-alloy steel specimens

Fig. 18. The micropits are often associated with cracks, as seen in Fig. 18; however, these are surface cracks in the oxide scale that do not extend into the material. None of the examined specimens showed any evidence that fatigue cracks nucleate preferentially at the micropits. Typical secondary fatigue cracks on the descaled surfaces of A06-Gr B and A533-Gr B specimens are shown in Fig. 19. Several corrosion pits and cavities created by dissolution of inclusions are visible on the surface and seem to be associated with the crack. However, there is no indication that the crack actually nucleated at any of these sites. The cracks appear to encounter and pass through these corrosion pits or through stringers of inclusions. Examination

of the fatigue specimens indicates that irrespective of environment, cracks in carbon and low-alloy steels nucleate along slip bands, carbide particles, or at the ferrite/pearlite phase boundaries. Examples of such cracks in a carbon steel specimen are shown in Fig. 20.

The metallographic examination was complemented by measuring the cracking frequency for fatigue specimens tested in different environments. Figure 21 shows plots, as a function of strain, of the number of cracks along longitudinal sections of the gage length of A106-Gr B and A533-Gr B specimens tested at two different strain rates in air, simulated PWR, and high-DO water. In all cases, the number of cracks represent the average value along a 7 mm gage length. The results show that with the exception of the low-alloy steel tested in simulated PWR water, environment has no effect on the frequency of cracks. For similar loading conditions, the number of cracks in the specimens tested in air and oxygenated water with 0.8 ppm DO are

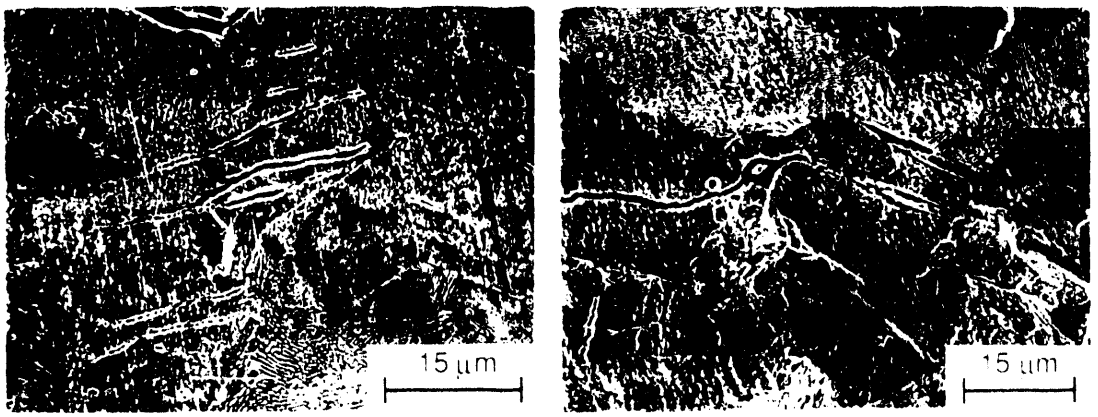

Figure 20. Nucleation of cracks along slip bands, carbide particles, and ferrite/pearlite phase boundaries of the carbon steel fatigue specimen

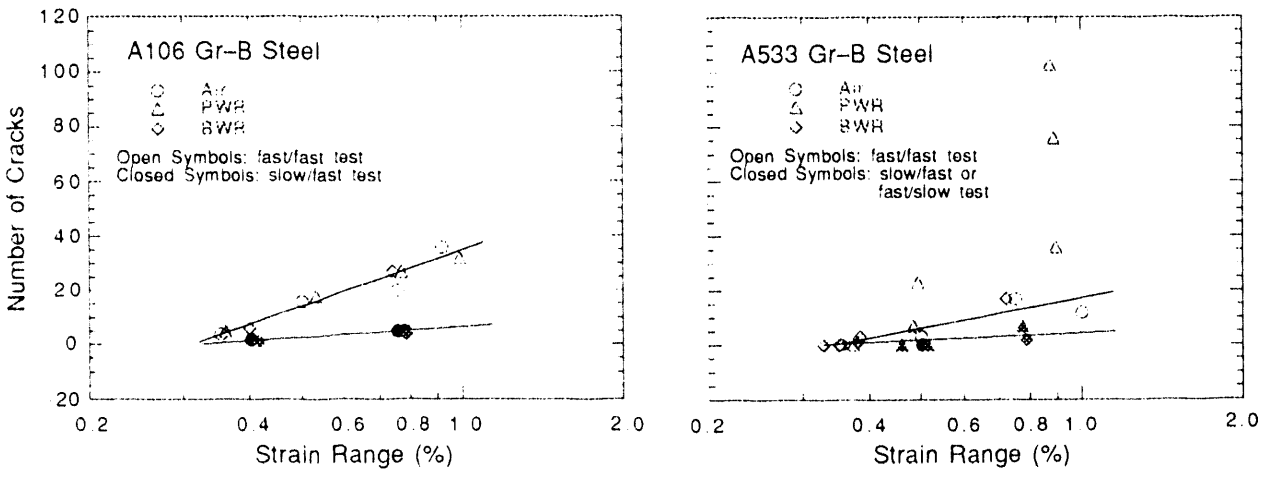

Figure 21. Number of cracks along a longitudinal section of the fatigue speciemns tested in different environments

identical, although fatigue life is a factor of ≈8 lower in water. If the reduction in life is caused by enhanced crack nucleation, the specimens tested in high DO water should show more cracks.

The low-alloy steel specimens tested in either simulated PWR water or deionized water with <10 ppb DO show a significantly higher frequency of cracks, although their fatigue life is only marginally lower than that in air. These cracks most likely are caused by hydrogen produced by the corrosion reaction. The frequency of cracks is higher only in the low-alloy steel and not in carbon steel because of structural differences; the low-alloy steel has high tensile strength and consists of tempered bainitic structure.

The contributions of environment to crack nucleation were further evaluated by conducting exploratory tests. Figure 22 shows the fatigue life of A106-Gr B steel in air (dashed line) and in high-DO water at 0.4 and 0.004%/s strain rates (circle and diamond symbols, respectively). A fatigue specimen was preexposed at 288°C for 100 h in water with 0.6 ppm DO and then tested in air at 0.4% total strain range. At this strain range, nearly half the fatigue life may be spent in crack nucleation. Fatigue life should be reduced if surface micropits facilitate crack nucleation; life of this specimen is identical to that of an unoxidized specimen. Similar behavior was observed for a preoxidized A533-Gr B specimen tested at 0.5% strain range. It is possible that the high DO and slow strain rate are also needed to influence crack nucleation. This possibility was checked by first testing a specimen in high-DO water at 0.4% strain range and 0.004%/s strain rate for 570 cycles (≈25% of the life at these loading conditions) and then testing in either air or water environment at 0.4%/s strain rate. Fatigue life of these tests should be reduced if crack nucleation contributes in any way to environmental effects. Once again, no reduction in life is observed. These results suggest that the reduction in fatigue life in oxygenated water is primarily due to environmental effects on fatigue crack propagation. Environment has little or no effect on crack nucleation.

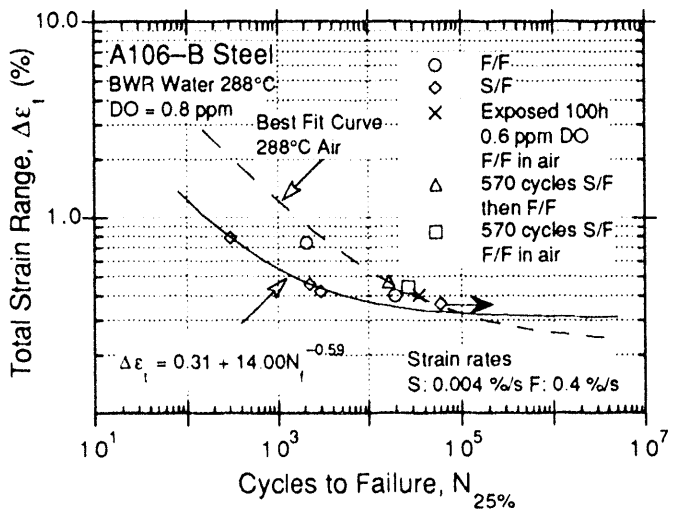

Figure 22.
Environmental effects on nucleation of fatigue crack

4 Conclusions

The fatigue behavior of A106–Gr B carbon steel and A533–Gr B low–alloy steel has been investigated in oxygenated water and in air. The results confirm the significant reduction in fatigue life and strong dependence on strain rate. For both steels, fatigue life in oxygenated water decreases with decreases in strain rate or increases in DO. The effects of strain rate on fatigue life saturate at some low value of strain rate, e.g., between 0.0004 and 0.001%/s in oxygenated water with ≈0.8 ppm DO. The actual value of saturation strain rate may vary with DO and sulfur content of the steel. The results show that although the cyclic stress–strain and cyclic–hardening behavior of carbon and low–alloy steels are distinctly different, there is little or no difference in susceptibility to environmental degradation of fatigue life of these steels, when sulfur levels are comparable. The A106–Gr B carbon steel exhibits pronounced dynamic strain–aging, whereas strain aging effects are modest in the A533–Gr B low–alloy steel.

A detailed examination of the gage surfaces of the specimens was conducted to investigate the role of high–temperature oxygenated water on fatigue crack nucleation. The results suggest that an oxygenated–water environment has no effect on the nucleation of cracks. All specimens tested in water showed surface micropitting, due to either corrosion of the material in oxygenated water or selective dissolution of MnS or other inclusions. However, there is no indication that a fatigue crack nucleated at any of the surface micropits. Examination of the fatigue specimens indicates that irrespective of environment, cracks in carbon and low–alloy steels nucleate along slip bands, carbide particles, or at the ferrite/pearlite phase boundaries.

Acknowledgments

The authors are grateful to W. F. Burke, J. C. Tezak, T. M. Galvin, and P. L. Torres for their contributions to the experimental effort in this program. This work was supported by the Office of Nuclear Regulatory Research of the U.S. Nuclear Regulatory Commission, under FIN Number A2212; Program Manager: Dr. J. Muscara.

References

1. *Criteria of Section III of the ASME Boiler and Pressure Vessel Code for Nuclear Vessels*, The American Society of Mechanical Engineers, United Engineering Center, New York, Library of Congress Catalog No. 56–3934 (1989).

2. Tentative Structural Design Basis for Reactor Pressure Vessels and Directly Associated Components (Pressurized, Water Cooled Systems), PB 151987, U.S. Department of Commerce, Office of Technical Service, 1 Dec. 1958 Revision.

3. D. A. Hale, S. A. Wilson, E. Kiss, and A. J. Gianuzzi, Low Cycle Fatigue Evaluation of Primary Piping Materials in a BWR Environment, GEAP–20244, U.S. Nuclear Regulatory Commission (Sept. 1977).

4. D. A. Hale, S. A. Wilson, J. N. Kass, and E. Kiss, "Low Cycle Fatigue Behavior of Commercial Piping Materials in a BWR Environment," *J. Eng. Mater. Technol.* **103**, 15–25 (1981).

5. S. Ranganath, J. N. Kass, and J. D. Heald, "Fatigue Behavior of Carbon Steel Components in High-Temperature Water Environments," in *Low-Cycle Fatigue and Life Prediction*, ASTM STP 770, C. Amzallag, B. N. Leis, and P. Rabbe, eds., American Society for Testing and Materials, Philadelphia, PA, pp. 436–459 (1982).

6. J. B. Terrell, *Fatigue Life Characterization of Smooth and Notched Piping Steel Specimens in 288°C Air Environments*, NUREG/CR-5013, MEA-2232 (May 1988).

7. J. B. Terrell, "Effect of Cyclic Frequency on the Fatigue Life of ASME SA-106-B Piping Steel in PWR Environments," *J. Mater. Eng.* **10**,193–203 (1988).

8. P. D. Hicks, in *Environmentally Assisted Cracking in Light Water Reactors: Semiannual Report October 1990—March 1991*, NUREG/CR-4667 Vol. 12, ANL-91/24, pp. 3–18 (Aug. 1991).

9. P. D. Hicks and W. J. Shack, Fatigue of Ferritic Steels, in *Environmentally Assisted Cracking in Light Water Reactors, Semiannual Report, April–September 1991*, NUREG/CR-4667 Vol. 13, ANL-92/6, pp. 3–8 (March 1992).

10. O. K. Chopra, W. F. Michaud, and W. J. Shack, "Fatigue of Ferritic Steels," in *Environmentally Assisted Cracking in Light Water Reactors, Semiannual Report, October 1992-March 1993*, NUREG/CR-4667 Vol. 16, ANL-93/27, pp. 3–19 (September 1993).

11. M. Higuchi and K. Iida, "Fatigue Strength Correction Factors for Carbon and Low-Alloy Steels in Oxygen-Containing High-Temperature Water," *Nucl. Eng. Des.* **129**, 293–306 (1991).

12. K. Iida, H. Kobayashi, and M. Higuchi, *Predictive Method of Low Cycle Fatigue Life of Carbon and Low Alloy Steels in High Temperature Water Environments*, NUREG/CP-0067, MEA-2090, Vol. 2 (April 1986).

13. N. Nagata, S. Sato, and Y. Katada, "Low-Cycle Fatigue Behavior of Low-Alloy Steels in High-Temperature Pressurized Water," in *Transactions of the 10th International Conf. on Structural Mechanics in Reactor Technology*, Vol. F, A. H. Hadjian, ed., American Association for Structural Mechanics in Reactor Technology, Anaheim, CA (1989).

14. S. Majumdar, O. K. Chopra, and W. J. Shack, *Interim Fatigue Design Curves for Carbon, Low-Alloy, and Austenitic Stainless Steels in LWR Environments*, NUREG/CR-5999, ANL-93/3 (April 1993).

15. T. A. Prater and L. F. Coffin, "The Use of Notched Compact-Type Specimens for Crack Initiation Design Rules in High-Temperature Water Environments," in *Corrosion Fatigue: Mechanics Metallurgy, Electrochemistry, and Engineering*, ASTM STP 801, T. W. Crooker and B. N. Leis, eds., American Society for Testing and Materials, Philadelphia, pp. 423–444 (1983).

16. T. A. Prater and L. F. Coffin, "Notch Fatigue Crack Initiation in High Temperature Water Environments: Experiments and Life Prediction," *J. of Pressure Vessel Technol.*, Trans. ASME, **109**, 124–134 (1987).

17. M. O. Speidel and R. M. Magdowski, "Stress Corrosion Cracking of Nuclear Reactor Pressure Vessel Steel in Water: Crack Initiation versus Crack Growth," *Corrosion 88*, Paper No. 283, St. Louis, Mo. (March 1988).

18. F. P. Ford and P. L. Andresen, "Stress Corrosion Cracking of Low-Alloy Pressure Vessel Steel in 288°C Water," in *Proc. 3rd Int. Atomic Energy Agency Specialists' Meeting on Subcritical Crack Growth*, NUREG/CP-0112, Vol. 1, pp. 37–56 (August 1990).

19. P. M. Scott and D. R. Tice, "Stress Corrosion in Low-Alloy Steels," *Nucl. Eng. Des.* **119**, 399–413 (1990).

20. W. H. Cullen, "The Effects of Sulfur Chemistry and Load Ratio on Fatigue Crack Growth Rates in LWR Environments," in *Proc. of the 2nd Int. Atomic Energy Agency Specialists' Meeting on Subcritical Crack Growth*, NUREG/CP-0067, MEA-2090, Vol. 2, pp. 339–355 (April 1986).

21. J. D. Atkinson, J. H. Bulloch, and J. E. Forrest, "TA Fractographic Study of Fatigue Cracks Produced in A533B Pressure Vessel Steel Exposed to Simulated PWR Primary Water Environments," in *Proc. of the 2nd Int. Atomic Energy Agency Specialists' Meeting on Subcritical Crack Growth*, NUREG/CP-0067, MEA-2090, Vol. 2, pp. 269–290 (April 1986).

22. W. A. Van Der Sluys and D. S. DeMiglio, "An Investigation of Fatigue Crack Growth in SA508-2 in a 288°C PWR Environment by a Constant ΔK Test Method," in *Proc. Int. Atomic Energy Agency Specialists' Meeting on Subcritical Crack Growth*, NUREG/CP-0044, MEA-2014, Vol. 1, pp. 44–64 (May 1983).

23. J. H. Bulloch, "A Review of the Fatigue Crack Extension Behavior of Ferritic Pressure Vessel Materials in Pressurized Water Reactor Environments," *Res. Mechanica* **26**, 95–172 (1989).

24. T. F. Kassner, W. J. Shack, W. E. Ruther, and J. H. Park, "Environmentally Assisted Cracking of Ferritic Steels," in *Environmentally Assisted Cracking in Light Water Reactors: Semiannual Report, April–September 1990*, NUREG/CR-4667, Vol. 11, ANL-91/9, pp. 2–9 (May 1991).

25. D. D. Macdonald, S. Smialowska, and S. Pednekar, *The General and Localized Corrosion of Carbon and Low-Alloy Steels in Oxygenated High-Temperature Water*, NP-2853 (February 1983).

26. J. Kuniya, H. Anzai, and I. Masaoka, "Effect of MnS Inclusions on Stress Corrosion Cracking in Low-Alloy Steels," *Corrosion*, Vol 48, No. 5, 419–425 (1992)

END

DATE
FILMED
3/7/94